Metallomics

Accepted Manuscript

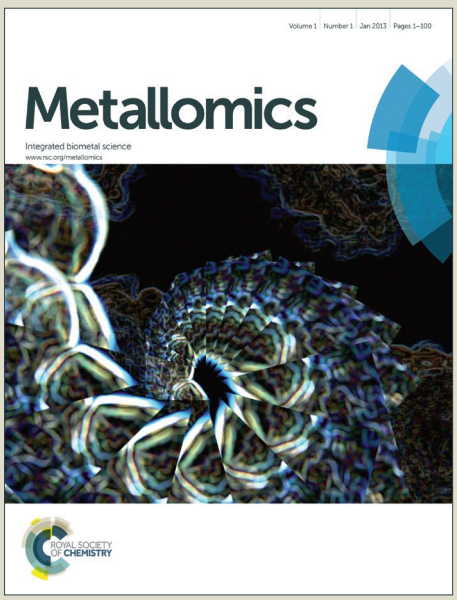

ROYAL SOCIETY OF CHEMISTRY

www.rsc.org/metallomics

Extravasation of Pt-based Chemotherapeutics – Bioimaging of their Distribution in Resectates by Laser Ablation-Inductively Coupled Plasma-Mass Spectrometry (LA–ICP-MS)

Alexander E. Egger[1,2], Christoph Kornauth[3], Werner Haslik[4], Stephan Hann[5], Sarah Theiner[2,6], Günther Bayer[3], Christian G. Hartinger[2,7], Bernhard K. Keppler[2,6], Ursula Pluschnig[8], Robert M. Mader[8]

[1]ADSI – Austrian Drug Screening Institute GmbH, Innsbruck, Austria

[2]Institute of Inorganic Chemistry, University of Vienna, Vienna, Austria

[3]Institute of Clinical Pathology, Comprehensive Cancer Center of the Medical University of Vienna, Vienna, Austria

[4]Department of Surgery, Division of Plastic and Reconstructive Surgery, Comprehensive Cancer Center of the Medical University of Vienna, Vienna, Austria

[5] Department of Chemistry, Division of Analytical Chemistry, University of Natural Resources and Life Sciences (BOKU), Vienna, Austria

[6]Research Platform 'Translational Cancer Therapy Research', University of Vienna, Vienna, Austria

[7] School of Chemical Sciences, University of Auckland, Auckland, New Zealand

[8]Department of Medicine I, Comprehensive Cancer Center of the Medical University of Vienna, Vienna, Austria

Correspondence to:

Robert M. Mader

Department of Medicine I, Clinical Division of Oncology

Comprehensive Cancer Center of the Medical University of Vienna

Währinger Gürtel 18-20

1090 Vienna, Austria

Phone: +431 40400 54660

Fax: +431 40400 60810

E-mail: robert.mader@meduniwien.ac.at

ABSTRACT

Platinum-based drugs (cisplatin, carboplatin and oxaliplatin) are widely used in cancer treatment. Although administered intravenously, accidental extravasations of infusions can occur. This may cause severe complications for the patient as the toxic platinum compounds likely persist in subcutaneous tissue. In high concentrations, platinum toxicity in combination with local thrombosis may result in tissue necrosis, eventually requiring surgical intervention.

To describe tissue distribution at the anatomic level, we quantified drug extravasation in cryosections of various tissue (muscle, nerve tissue, connective tissue, fat tissue) by means of quantitative laser ablation-inductively coupled plasma-mass spectrometry (LA–ICP-MS) and compared the resulting data with bulk analysis of microwave-assisted digestion of tissue samples followed by ICP-MS analysis.

Samples of three patients receiving systemic chemotherapy either via peripheral venous access or central access via port-a-cath® were analyzed. Pt was enriched up to 50-times in connective tissue when compared with muscle tissue or drain samples collected over five days. The large areas of subcutaneous fat tissue, showed areactive necrosis and average Pt concentrations (determined upon sample digestion) ranged from 0.2 µg/g (therapy with 25 mg/m^{2}cisplatin, four weeks after peripheral extravasation) to 10 µg/g (therapy with 50 mg/m^2 oxaliplatin: four weeks after port-a-cath® extravasation). A peripheral nerve subjected to bioimaging by LA–ICP-MS showed a 5-times lower Pt concentration (0.2 µg/g) than the surrounding connective tissue (1.0 µg/g). This is in accordance with the patient showing no signs of neurotoxicity during recovery from extravasation side-effects. Thus, bioimaging of cutaneous nerve tissue may contribute to understand the risk of peripheral neurotoxic events.

INTRODUCTION

Extravasation of cytotoxics is referred to as the unintended instillation or leakage of drugs into the perivascular space or into the subcutaneous tissue during infusion and has been reported in 0.1-6.5% of cytotoxic infusions.[1] The local damage primarily depends on the toxicity of the extravasated compound and strongly on the amount of drug in the affected lesion.[2] Despite an ongoing discussion, there are three different classes of compounds with regard to their subcutaneous toxicity: i) non-vesicant substances (no local irritation), ii) irritant substances, which may cause local pain, swelling

and local irritations, but no necrosis, and iii) vesicant substances, which may result in ulcerations and necroses.[3] Severe extravasations of vesicants can lead to damage of soft tissue (muscles), tendons and nerves but also scar formation eventually requiring surgical interventions such as debridement with subsequent skin and tissue transplantation. Little is known about the mechanisms of acute toxicity in subcutaneous tissue, where severe cases present with early thrombosis in the affected lesion thus impairing the efflux of the toxic agents with the blood stream. In experimental studies, heparin has been used to mitigate the effect of the highly toxic agent doxorubicin.[4] As a consequence of impaired blood flow both the compound itself and the shortage of oxygen can potentiate the irreversible tissue damage as recently substantiated by angiographic monitoring of patients.[5] In this investigation, the blood flow in the central area of the affected lesion was predictive for the clinical outcome after extravasation of vesicants. The critical question about the relationship between tissue toxicity and local concentration of the cytotoxic agent has not been addressed so far neither is the mechanism of cutaneous toxicity fully understood. Even less is known about the distribution of extravasated agents within the affected lesion, particularly with a resolution at the anatomic level.
This might be of particular interest in a group of drugs, which have been classified as irritants as well as vesicants, *i.e.* platinum(II) compounds. These drugs are routinely used for treatment of a variety of cancer types including cancer entities difficult to treat such as lung, ovarian and advanced colorectal cancer. The first platinum(II) compound being worldwide approved, cisplatin, is considered to be a vesicant in concentrated solutions, whereas in dilutions it is qualified as an irritant only.[6] In the case of oxaliplatin, severe necrosis has been observed infrequently and carboplatin is the only established Pt(II)-based drug not being toxic to tissue.[7] Studying the distribution of these agents in affected tissue might, therefore, provide relevant information to correlate local toxicity with the amount of extravasated drug.

To address these questions, imaging techniques based on mass spectrometry[8, 9] or micro X-ray fluorescence (μ-XRF)[10, 11] are best suited, as they allow to monitor the spatially-resolved elemental distribution at histological levels in the μm range. Laser ablation-inductively coupled plasma-mass spectrometry imaging (LA–ICP-MS imaging) and μ-XRF allow detection and quantification of the element of interest independent from the binding partner. Thus, the applied drug and all its metabolites are recorded at the same time as a measure for total drug loading in the respective tissue. In the case of LA-ICP-MS the outstanding spatial resolution of the laser (spot-size in the low μm scale) is combined with the sensitivity of mass spectrometric detection. In contrast to LA-ICP-MS, μ-XRF is non-destructive as the sample is irradiated with X-rays followed by registration of the emitted, element-specific radiation. Its broad field of application ranges from geological and archaeological to biological samples including intracellular visualization of Pt upon cisplatin treatment of cells.[11, 12] However, access to a synchrotron facility is required and measurement time is

longer compared to LA-ICP-MS imaging. Recently, both techniques were compared regarding sensitivity using sections of *Daphnia magna*. Both techniques achieved limits of detection in the low µg/g range, but depending on the element of interest, either LA-ICP-MS (e.g. for Zn) or µ-XRF (e.g. for S) was better suited.[13]

In our study we applied LA-ICP-MS imaging, and its general workflow is conducted in the following manner: cryosections of tissues are placed into an ablation chamber, where a focused, high energetic laser beam completely ablates the tissue in parallel line scans and the resulting aerosol is transferred to the ICP-MS. Argon plasma is used for atomization and ionization. Independent from the original binding partners, the resulting (metal) ions are separated by a mass-analyzer and detected. Subsequently, the metal distributions are superimposed to stained tissue sections providing a new dimension of data, not accessible by classical staining procedures, thus supporting histological interpretation (Figure 1).[14]

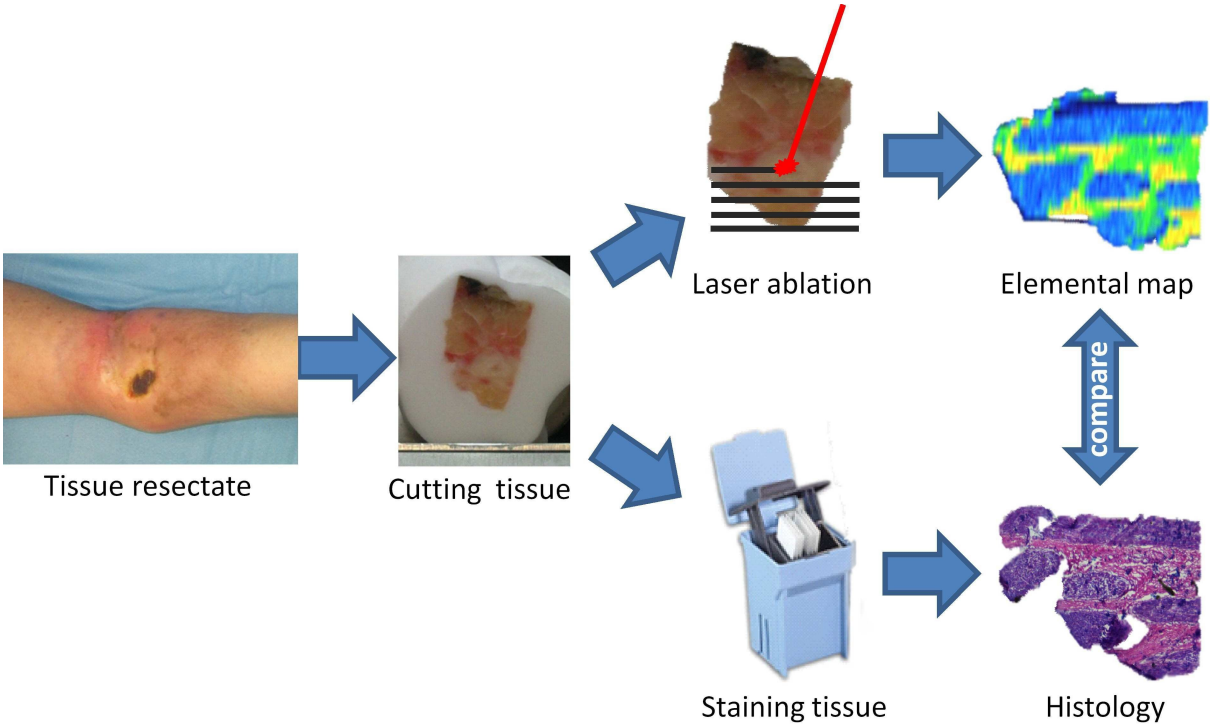

Figure 1: Workflow for bioimaging experiments based on mass spectrometry. Cryosections of the sample are prepared and subjected either to mass spectrometry imaging (e.g. LA–ICP-MS) or histologic staining procedures.

LA–ICP-MS has already been applied to investigate metal distribution in brain tissue to improve the understanding of the development of neurodegenerative diseases,[15, 16] to monitor the fate of Au or Ag containing nanoparticles in cells,[17] to study the Pt distribution in kidneys upon treatment of rodents with the nephrotoxic complex cisplatin[18] or to obtain a more detailed picture on pharmacokinetics in preclinical metal-based anticancer drug development.[19] In the field of patient related applications, LA–ICP-MS has recently been applied to monitor the drug uptake in peritoneal carcinosis treated by hyperthermic intraperitoneal chemotherapy (HIPEC) with cisplatin and

oxaliplatin[20, 21] and a new strategy for quantitative LA–ICP-MS used a mesothelioma sample (treated with cisplatin) as proof of principle.[22]

In this investigation, we apply LA–ICP-MS imaging for the first time to quantify the Pt burden in various tissue types of three patients upon extravasation of cisplatin or oxaliplatin chemotherapy at microscopic levels. In addition, we compare this technique with established protocols for metal-based bulk analysis by microwave-assisted digestion preceding quantification by means of ICP-MS and we discuss the entire data set in relation to the clinical outcome.

EXPERIMENTAL

Patient details and sampling. Patients underwent intravenous anticancer Pt-based chemotherapeutic treatment in the Vienna General Hospital / Medical University of Vienna (see Table 1). Three patients experiencing an extravasation were subject to immediate surgical intervention (patient 1) or four weeks thereafter (patients 2 and 3). Samples were taken for quantitative bulk analysis of Pt concentrations as well as spatially resolved visualization of the Pt distribution thereof.

Table 1: Dosage of the chemotherapeutic Pt compound and overview of the extravasation event

Patient	Chemotherapeutic drug and dosage	Location of extravasation	Surgical intervention after extravasation
Patient 1 (male)	Cisplatin: 25 mg/m^2 or 50 mg absolute dose	Port-a-cath, subclavicular right	Immediately
Patient 2 (male)	Oxaliplatin: 50 mg/m^2 or 107 mg absolute dose	Port-a-cath, Subclavicular left	4 weeks
Patient 3 (female)	Cisplatin: 25 mg/m^2 or 41.5 mg absolute dose	Cubital vein forearm	4 weeks

In detail, four tissue samples surrounding the chamber of the port from patient 1 (G1, G2, G3, G5) were collected for bioimaging with LA–ICP-MS. In addition, aliquots from the intraoperative rinsing solution (rinsing with 100, 200 and 300 ml of 0.9% NaCl) as well as daily aliquots from post-operative exsudate (up to 5 days) were taken.

In patient 2, necrotic skin and soft tissue (19 × 13.5 × 3.5 cm) from the left pectoral region containing the Port-a-cath® System was resected. Thereof, a slice including the necrotic area was dissected into small pieces (Figure S5, supporting information). Samples were processed using microwave digestion followed by solution-based quantification of Pt by means of ICP-MS.

In patient 3, cisplatin extravasation caused necrosis in the cubital region and left forearm, which required surgical intervention upon four weeks. Ulcerated skin, soft tissue and nerve tissue from the left cubita were resected (14 × 12 × 3.5 cm). Cryosections of the ulcerous area were prepared for Pt-imaging, for histological staining (hematoxylin-eosin stain) to assign Pt distribution to anatomic structures, and for histopathologic studing of necrosis. The neighboring area was reduced to small pieces and quantification of Pt was performed by ICP-MS upon microwave-assisted digestion as an independent technique for quantification of Pt in tissue. In addition, cryosections were prepared in a distance of approx. 2.5 cm from the ulcus to evaluate signs of necrosis and the Pt concentration was determined in adjacent samples by ICP-MS. A cutaneous nerve, located in the resectate, was

prepared for quantitative LA–ICP-MS imaging. All samples were stored at -80°C upon surgical removal until cryosectioning took place.

Microwave-assisted digestion of tissue samples and solution-based ICP-MS. An ETHOS microwave digestion system (MLS, Leutkirch, Germany), equipped with an MR-10 rotor for 30 QS-3 teflon tubes was used. Prior to tissue sample digestion, all tubes were cleaned with equal volumes of water and sub-boiled nitric acid (≥65%, p.a., Fluka, Buchs, Switzerland) at 180 °C for 12 min under temperature control of one vessel (Table S1 for detailed parameters). Subsequently, the samples with a moist mass of 10–30 mg were digested under the same conditions as the purification was performed. Samples were diluted with Milli-Q water (18.2 MΩ cm, Milli-Q Advantage, Darmstadt, Germany) yielding a nitric acid concentration of approx. 3.5% and Pt concentrations not exceeding 15 ng/g. An ICP-MS instrument (Agilent 7500ce, Waldbronn, Germany) equipped with a CETAC ASX-520 autosampler (Nebraska, USA) and a MicroMist nebulizer at a sample uptake rate of approximately 0.25 ml/min was used for quantification of Pt, and Re served as internal standard (both obtained from CPI International (USA). Experimental parameters are summarized in Table 2. Data processing was conducted with the MassHunter software package (Agilent, Workstation Software, Version B.01.01, 2012).

Table 2: Parameters for the quantification of liquid samples by ICP-MS and for the hyphenation with a laser ablation system

	ICP-MS	**LA–ICP-MS**
RF Power [W]	1500	1350
Cones	Ni	Ni
Registered Isotopes	^{185}Re, ^{194}Pt, ^{195}Pt	^{195}Pt
Dwell time [s]	0.1	0.1
Replicates	10	-
Carrier gas [l/min]	0.9	1.0
Make up gas [l/min]	0.2	-
Plasma gas [l/min]	15	15

Determination of Pt in drain. Drain samples were analyzed for their platinum content via ICP-MS after closed vessel microwave digestion. Sample preparation and measurement were carried out in clean rooms class 100000 and 10000, respectively. As the total dissolved solid content of the investigated samples was varying, we applied the concept of isotope dilution analysis utilizing

platinum enriched in ^{196}Pt (97.25% enrichment) as a spike. An accurately weighed amount of 100-300 mg drain sample was transferred to a microwave liner of the microwave oven (MLS 1200 Mega controlled by a Mega 240 terminal, Milestone-MLS GmbH, Leutkirch, Germany). Afterwards, 3 ml of a 1:3 mixture of doubly sub-boiled HNO_3 and sub-boiled HCl (*aqua regia*) and 0.5 ml of ultrapure H_2O_2 (VWR) were added together with approx. 200 mg of the exactly weighed Pt spike solution containing approx. 100 ng/g ^{196}Pt. The concentration of the spike was determined by reverse isotope dilution analysis. The detailed procedure used for spike preparation and quantification has been described elsewhere.[23] Digestion was performed applying a microwave program as follows: 2 min/250 W, 2 min/0 W, 6 min/250 W, 5 min/400 W, 5 min/600 W. After cooling, the acidic solutions were transferred to PFA vessels, evaporated on a hot plate to approx. 0.5 ml and filled to 5 ml using 1:50 diluted sub-boiled HCl. Determination of total platinum concentrations was performed using a high-resolution ICP-sector field mass spectrometer (Element 2, Thermo Fisher Scientific, Bremen, Germany). After a first screening of the samples the solutions were appropriately diluted to match the linear dynamic range of the ICP-SFMS system. The limit of detection was determined by measurement of n=6 digestion blanks, resulting in a procedural limit of detection (3s-criterion) of 0.4 ng/g Pt in the original samples. Accuracy and repeatability of the quantification and measurement procedures were determined by repetitive measurements of 5 independently spiked CLMS-3 certified reference solutions (SPEX CertiPrep, Metuchen, NJ, USA) revealing a bias of 4.8% and a relative standard deviation of 0.07%. The total combined uncertainty of the overall procedure (including the digestion step) was 5.0%.

Bioimaging by LA–ICP-MS imaging. Bioimaging, including preparation of matrix-matched standards for quantification, was performed according to a previously published procedure.[19] Briefly, tissue homogenates of pig liver were spiked with Pt standard solutions yielding final concentrations of 1 to 45 µg/g. The platinum concentrations of the tissue standards were validated by microwave-assisted digestion followed by quantification using ICP-MS. The experimentally determined values were used for setting up calibration curves for LA–ICP-MS experiments (Figure S1). Consecutively, the homogenized tissue standards and human tissue samples were cryosectioned (20 µm) with a cryotom (Microm HM 550, Thermo Fisher) and analyzed by means of LA–ICP-MS. Standards (line scans of 2 mm per standard level) were analyzed prior and after the human samples to monitor instrumental drift. Laser ablation was performed with a Nd:YAG solid state laser (NWR 213,ESI, Fremont, CA, USA) at a wavelength of 213 nm, equipped with a 2 volume ablation cell to reduce wash out time. The laser beam path was equipped with a square-shaped laser spot table ensuring a constant delivery of energy onto the moving sample throughout the entire diameter of the laser beam. An optical sample map of the region of interest was generated and the ablation pattern

(parallel line scans) was defined. The laser was operated at 10 Hz, with a fluence in the range of 2.1 to 2.5 J/cm², a spot size of 70 µm, a scan speed of 40 µm/s and spacing of 10 µm between the lines. The ablated material was transferred to the ICP-MS with He (quality 5.0) at a flow rate of 400 ml/min. Operational parameters for the ICP-MS under imaging conditions are summarized in Table 2.

Data analysis. The recorded files were imported into Iolite (Version 2.15)[24] as an add-on to Igor Pro (Wavemetrics, Igor Pro 6.22a) and processed according to the provided manual (Iolite User Manual, Version 2.0).[25] The aspect ratio of the image was set according to the dimensions of the ablated area to obtain accurately shaped pictures. GIMP (Version 2.8.6) was used to assemble the optical image and the corresponding Pt distribution. In the case matrix-matched standards were measured for quantitative bioimaging, the concentration of each standard was assigned in the scale bar of the image to the corresponding average counts.[19]

Assessment of average concentrations per tissue type at microscopic level by means of LA–ICP-MS is based on a greyscale color scheme for image export in iolite, providing a linear correlation between the grey value (in the range of 0 and 255) and the registered CPS ^{195}Pt. In addition, the registered counts per second (CPS) correlate with the concentration of the ablated standards, enabling conversion of grey values to concentration (expressed in µg/g) using ImageJ (Version 1.48v).[26] Upon calibration, Pt distributions corresponding to the same tissue type were combined to one region of interest and its average concentration was read out using the histogram function of ImageJ.

RESULTS AND DISCUSSION

Validity of the bioimaging data. Estimating validity of quantitative bioimaging data is challenging as neither tissue standards nor certified reference materials for LA–ICP-MS of biological samples are available. Thus, matrix-matched standards based on pig liver homogenates were prepared and their concentration was verified independently using microwave-assisted digestion followed by ICP-MS analysis. The concentrations obtained using both methods are in good agreement (detailed comparison in Table S2). In terms of quantitative LA–ICP-MS, we recently reported that internal standards such as ^{115}In, ^{185}Re or ^{13}C neither improve precision nor accuracy of spatially-resolved Pt or Ru determinations significantly.[19] However, in the absence of an internal standard, other strategies to monitor instrumental drifts in the case of long lasting bioimaging experiments (up to several hours) were applied: standards were measured at the beginning and at the end of the laser ablation experiment in order to estimate long-term instrumental drift, which did not exceed 15% in any

experiment. In case sufficient sample material was available (patient 3), the quantification of Pt in the sample was performed by an LA-independent methodology using microwave-assisted digestion/ICP-MS of neighboring samples. Analysis of the necrotic area of patient 3 was conducted in the following manner: The median concentration of Pt, determined by LA–ICP-MS imaging and using ImageJ for calculations was found to be 0.33 µg/g and the first and third quartile of the distribution were determined to 0.20 µg/g and 0.53 µg/g, respectively (Figure S6). In order to validate the concentration in an independent manner, five samples, adjacent to the sample analyzed by LA-ICP-MS imaging, were subjected to microwave-assisted digestion and consecutive ICP-MS analysis (Figure 3). Their average concentration was calculated to 0.20±0.11 µg/g, thus supporting the validity of the concentration determined by bioimaging.

Pt distribution in tissue and kinetics of Pt release after port-a-cath® extravasation. Patient 1 underwent immediate surgical intervention on the day of cisplatin extravasation (rinsing and port explantation including a small tissue cuff). In order to quantify the Pt burden in tissue, intraoperative rinse and drain solutions over 5 days as well as tissue samples surrounding the extravasate were analyzed. Four tissue samples were subjected to quantitative LA–ICP-MS imaging (Figure 2, Figure S2). Three of them contained subcutaneous fat and connective tissue (G1, G2, G3), while the fourth also contained small parts of the pectoralis major muscle (G5). All tissue samples exhibited minimal, focal lymphoidic infiltrations.

The high spatial resolution of the applied imaging technique allowed assignment of concentrations to the observed different types of tissue at microscopic scales. Connective tissue accumulated highest amounts of Pt in all samples while lower concentrations in muscle and fat tissue were observed. ImageJ was used to calculate the average concentrations of Pt for each tissue type in sample G1 and G5 (see Figure S3 and S4, respectively for the regions on interest, which calculations are based on). In sample G1, average Pt concentrations of 2.2 and 29 µg/g were found in fat and connective tissue, respectively, and in sample G5, 56 and 7.5 µg/g Pt were recorded in connective tissue and muscle tissue. However, it is important to mention that the Pt concentration in fat tissue may be underestimated in the case of bioimaging (see results and discussion of patient 3).

In all samples analyzed (*cf.* also Figure S2 for corresponding histograms and regions of interest) Pt was found to be approx. 10-fold increased in connective tissue, compared with muscle and fat tissue.

In a next step, we compared the Pt concentration in tissue with those found in liquid samples. The Pt concentration in tissue was approx. two orders of magnitude higher than in liquid samples taken during rinsing (Table 3). This is explained by stepwise rinsing with volumes of 100 ml leading to

diluted samples, thus only the concentration course in dependence of the rinsed volume (0-300 ml) or time period since surgical intervention (one to five days) is a meaningful interpretation. Intraoperative sample collection of the rinsing solutions revealed a platinum concentration of ~0.4 µg/g prior to rinsing, which decreased to 0.121±0.006 µg/g upon rinsing with a total volume of 300 ml of 0.9% NaCl. The Pt levels in drain solutions collected each day increased continuously over time from 0.417 µg/g at day 1 to 1.470 µg/g on the fifth post-operative day (Table 3). Thus, removal of Pt from the affected lesion bed was found to start with time delay.

Table 3: Concentration of Pt determined in intraoperatively retrieved samples prior to rinsing the port-a-cath (I) and upon rinsing with the stated total volume of 0.9% NaCl (II to IV). Subsequently, post-operative kinetics of Pt secretion over 5 days was studied in drain samples of patient 1.

Sample	Pt [µg/g]
I (0 ml)	0.383±0.019
II (100 ml)	0.118±0.006
III (200 ml)	0.185±0.009
IV (300 ml)	0.121±0.006
Drain Day 1	0.417±0.021
Drain Day 2	0.684±0.034
Drain Day 3	1.170±0.059
Drain Day 4	1.420±0.071
Drain Day 5	1.470±0.074

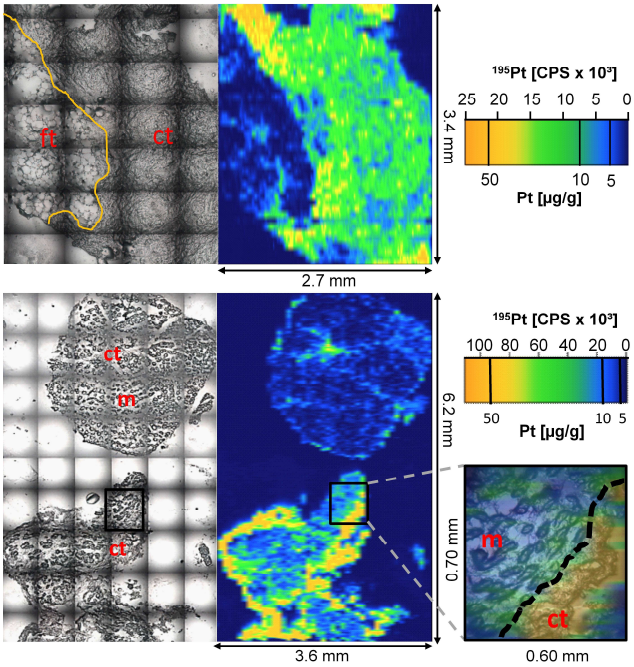

Figure 2: Patient 1, sample G1 (top) and G5 (bottom). Matrix-matched standards were used to estimate spatially-resolved concentrations of Pt in samples. The greyscale pictures were recorded prior to ablation of the tissue, thus best correlation with Pt distribution is maintained. Fatty tissue (ft), connective tissue (ct) and muscle (m) were analyzed. The enlarged area (bottom right) of a borderline between connective tissue and muscle, measuring 0.6 × 0.7 mm, shows the spatial resolution of the method close to cellular level.

Samples from the second extravasation event (patient 2) *via* a port-a-cath® consisted of a disk of subcutaneous fat tissue, which was surgically removed 4 weeks after administration of oxaliplatin (dose: 50 mg/m^2). Cryosections maintaining the histologic structures (mainly fat tissue) could not be obtained, thus the analysis of samples was based on microwave-assisted digestion followed by ICP-MS analysis. A scheme of the samples, their location within the disk and their concentrations is given in Figure S5. Samples located in proximity to the base of the port, exhibited highest concentration of Pt (up to 44 µg/g) and average concentrations of a slice (*i.e.* stripes of approx. 1 cm in width containing the entire layer from the skin to the fascia) were highest at the location of the port (11-16 µg/g) and decreased with distance to approx. 3 µg/g. At first glance, this is in good agreement with the reported concentration in fat tissue of the first patient investigated (2.2 µg/g). However, the patients were treated with different drugs and dosages (50 mg/m^2 oxaliplatin vs. 25 mg/m^2 cisplatin, respectively), surgical intervention took place immediately or upon four weeks, LA–ICP-MS may underestimate Pt concentrations when fat tissue is investigated (see below), and sample material of patient 1 was insufficient to apply microwave-assisted digestion followed by ICP-MS analysis.

Pt distribution in tissue upon peripheral extravasation (cubital vein). The third patient received cisplatin via a peripheral venous access and surgical intervention was required four weeks upon extravasation due to ulceration. A disk of the resectate, covering the ulcerous area, and its sampling for microwave digestion, histologic evaluation and LA–ICP-MS imaging is depicted in Figure 3 (top). Microwave-assisted digestion and quantification by ICP-MS of the samples revealed Pt concentrations of approx. 0.2 µg/g (Figure 3, bottom). A miniaturized version of the tissue section on which LA–ICP-MS was applied is included in the sketch, considering an identical color scheme and concentration limits. Thus, visual comparison between the reported concentrations obtained by these complementary techniques is justified to assess validity of the bioimaging procedure: orange colors of the digested samples are in accordance with the yellowish-reddish fine structures obtained by LA imaging.

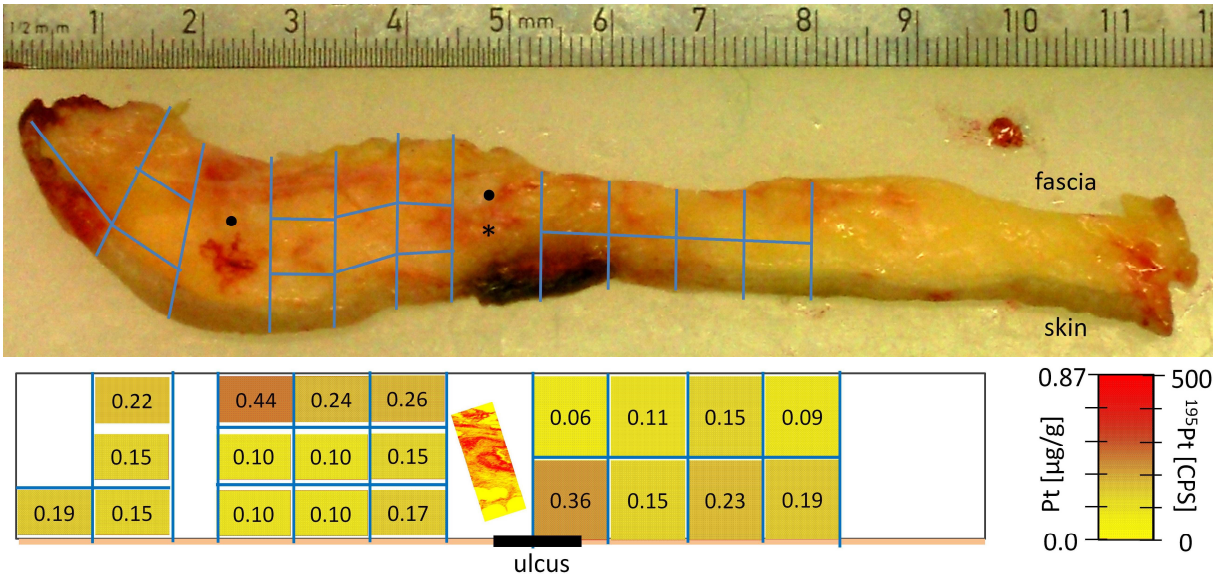

Figure 3: **Top**: Resectate of patient 3 was dissected into small pieces (blue lines) for quantitative determination of the average Pt concentration within the necrotic fat tissue. In addition, a sample (*) of the ulcerous region was used for quantitative laser ablation ICP-MS imaging of Pt. The remaining tissue samples, indicated by (•), were placed in formalin for histopathologic evaluation of necrosis in fat tissue. **Bottom**: Average concentrations of Pt (in µg/g) in tissue (determined in solution upon digestion) were highlighted with the color according to the scale bar. The colors of the miniaturized LA-ICP-MS image, compared with the adjacent samples, are in good accordance.

In a next step, the histology of areas containing similar Pt concentrations was investigated. Figure 4 depicts a greyscale image of the tissue section prior to ablation, the resulting Pt distribution within the section as well as a hematoxylin-eosin stained consecutive cryosection for improved histopathological assignment.

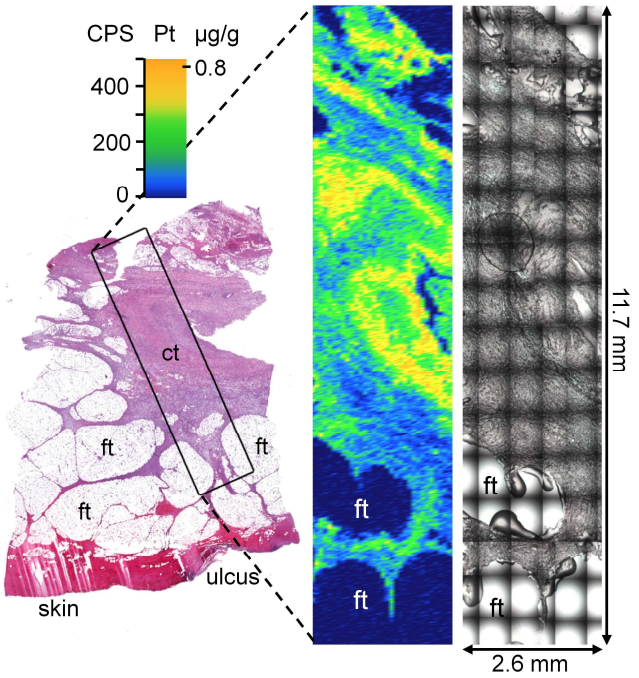

Figure 4: Pt distribution in the necrotic area of subcutaneous tissue. Greyscale image (right) was recorded prior to LA–ICP-MS. The resulting quantitative Pt distribution (middle) and a hematoxylin eosin stained consecutive slice (left) are shown to assign histological structures to the Pt distribution. The black rectangle indicates the ablated area. Fat tissue (ft) and connective tissue (ct) were analyzed.

The greyscale image (Figure 4, right), taken prior to ablation, exhibits confluent droplets of fat tissue (ft), which had already formed during cryosectioning of the tissue resulting in large tissue-free areas. Thus, LA–ICP-MS underestimated the Pt concentration in fat tissue (dark blue, corresponding to blank values), and microwave-assisted digestion preceding ICP-MS analysis gives more reliable concentrations of Pt in fat tissue (approx. 0.1-0.3 µg/g). Besides the fat tissue, a large region of necrotic connective tissue with blood vessels, necrotic fat tissue with foamy cells in close proximity to the ulcerous skin was subjected to bioimaging revealing Pt concentrations close to 1 µg/g. Histologic evaluation of formalin-fixed samples indicated with (•) in Figure 3 showed necrotic fat tissue with broad areas of areactive necrosis and only focal inflammatory reaction.

Neurotoxicity is one of the major adverse effects in platinum-based anticancer treatment after long-term application. Thus, a cutaneous nerve, embedded in the resectate, was subjected to bioimaging of Pt (Figure 5).

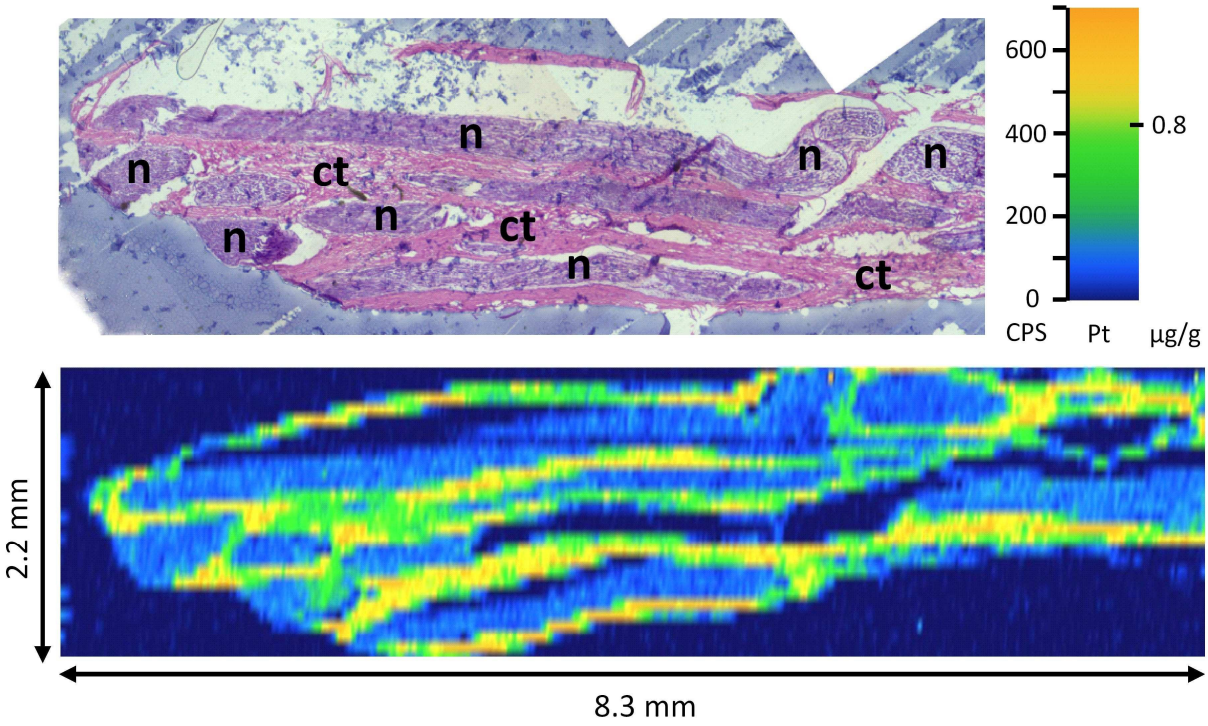

Figure 5: Cutaneous nerve obtained from patient 3, surgical resection four weeks upon extravasation. Hematoxylin-eosin stained section exhibits nerve tissue (n) and connective tissue (ct), top. The Pt distribution (bottom) correlates with histologic structures, revealing lower amounts in nerve tissue (blue) compared to connective tissue (green-orange).

Although four weeks elapsed between extravasation and surgical resection, considerable amounts of Pt were detected and correlated with histologic structures. The connective tissue surrounding the nerve fibers exhibited 5-times higher Pt levels than the nerve tissue. In detail (as calculated by ImageJ see Figure S7 for histograms and boxplots), the Pt median concentration was only 0.21 µg/g in nerve tissue, but 1.1 µg/g in the adjacent connective tissue, equipollent to the highest Pt levels of the entire resectate and in accordance with the Pt-levels found in connective tissue surrounding the

necrotic area (Figure 4). Notably, this concentration gradient between two neighboring tissue types maintained over weeks, indicating that the formed metabolites of cisplatin were unable to penetrate nerve tissue. This is in accordance with the clinical outcome of the patient, as no signs of neurotoxicity (*e.g.* sensory or motoric deficiency) were observed. Although this result is based solely on a case report, determination of the penetration of metal-based drugs in nerve tissue may become useful to relate neurotoxicity and local platinum levels in case of extravasation of Pt-based chemotherapeutics.

CONCLUSION

LA–ICP-MS imaging was applied to analyze tissue samples originating from three patients receiving Pt-based cancer treatment. These patients required surgical intervention after extravasation of the drug into the surrounding tissue. For the first time, we correlated the spatially-resolved Pt distribution in resectates with various (damaged) tissue types (muscle, fat tissue, nerve tissue, connective tissue) at a spatial resolution respecting the anatomic structures.

The Pt levels in tissue were significantly higher (10 to 50 times) than those in wound drains of the same person indicating high persistence of Pt in the affected lesion. Connective tissue exhibited higher concentrations of Pt than the neighboring muscle in samples originating from immediate surgical intervention. In the case of fat tissue, LA–ICP-MS is of limited value as confluent droplets of fat formed during sample preparation/storage resulting in underestimation of the Pt concentrations compared to solution-based analysis of the same samples. Even four weeks after extravasation, analysis of nerve tissue and surrounding connective tissue showed 5-times higher Pt amounts in connective tissue than in the neighboring nerve tissue, being in agreement with the patient's outcome (no signs of neurotoxicity).

Taken together, spatially-resolved visualization of Pt adds a new dimension in the interpretation of tissue sections, opens up the possibility to correlate histologic alterations with the amount of drug in tissue, and may be useful to establish a dose-response relationship in scenarios with local tissue damage.

ACKNOWLEDGMENT

C.G.H. is grateful for financial support provided by the Austrian Science Fund (Project number I496-B11). Gerlinde Grabmann is acknowledged for motivating discussions.

REFERENCES

1. G. Bertelli, *Drug Saf.*, 1995, 12, 245-255.
2. R. Rudolph, R. S. Stein and R. A. Pattillo, *Cancer*, 1976, 38, 1087-1094.
3. F. J. A. Perez, F. L. Garcia, A. Cervantes, A. Margulies, C. Vidall and F. Roila, *Annales of Oncology*, 2012, 23 Suppl 7, vii167-173.
4. I. Askar, M. K. Erbas and A. Gurlek, *Ann. Plast. Surg.*, 2002, 49, 297-301.
5. W. Haslik, U. Pluschnig, G. G. Steger, C. C. Zielinski, K. F. Schrogendorfer, J. Nedomansky, R. Bartsch and R. M. Mader, *PLoS One*, 2014, 9, e103649.
6. I. Mader, P. R. Fürst-Weger, R. M. Mader, E. Nogler-Semenitz and S. Wassertheurer, *Extravasation of Cytotoxic Agents*, Springer, Wien New York, 2 edn., 2010.
7. U. Pluschnig, W. Haslik, G. Bayer, A. Soleiman, R. Bartsch, W. Lamm, G. G. Steger, C. C. Zielinski and R. M. Mader, *Support. Care Cancer*, 2014, in press.
8. J. Liu and Z. Ouyang, *Anal Bioanal Chem*, 2013, 405, 5645-5653.
9. J. S. Becker and N. Jakubowski, *Chem. Soc. Rev.*, 2009, 38, 1969-1983.
10. C. J. Fahrni, *Curr. Opin. Chem. Biol.*, 2007, 11, 121-127.
11. M. West, A. T. Ellis, P. J. Potts, C. Streli, C. Vanhoof, D. Wegrzynek and P. Wobrauschek, *J. Anal. At. Spectrom.*, 2012, 27, 1603-1644.
12. K. G. Chen, J. C. Valencia, B. Lai, G. Zhang, J. K. Paterson, F. Rouzaud, W. Berens, S. M. Wincovitch, S. H. Garfield, R. D. Leapman, V. J. Hearing and M. M. Gottesman, *Proc. Natl. Acad. Sci. U. S. A.*, 2006, 103, 9903-9907.
13. D. S. Gholap, A. Izmer, B. De Samber, J. T. van Elteren, V. S. Šelih, R. Evens, K. De Schamphelaere, C. Janssen, L. Balcaen, I. Lindemann, L. Vincze and F. Vanhaecke, *Anal. Chim. Acta*, 2010, 664, 19-26.
14. S. J. Becker, *J. Mass Spectrom.*, 2013, 48, 255-268.
15. J. S. Becker, *Int. J. Mass spectrom.*, 2010, 289, 65-75.
16. Y. Ha, O. G. Tsay and D. G. Churchill, *Monatsh. Chem.*, 2011, 142, 385-398.
17. D. Drescher, C. Giesen, H. Traub, U. Panne, J. Kneipp and N. Jakubowski, *Anal. Chem.*, 2012, 84, 9684-9688.
18. E. Moreno-Gordaliza, C. Giesen, A. Lázaro, D. Esteban-Fernández, B. Humanes, B. Cañas, U. Panne, A. Tejedor, N. Jakubowski and M. M. Gómez-Gómez, *Anal. Chem.*, 2011, 83, 7933-7940.
19. A. E. Egger, S. Theiner, C. Kornauth, P. Heffeter, W. Berger, B. K. Keppler and C. G. Hartinger, *Metallomics*, 2014, 6, 1616-1625.

20. J. Bianga, A. Bouslimani, N. Bec, F. Quenet, S. Mounicou, J. Szpunar, B. Bouyssiere, R. Lobinski and C. Larroque, *Metallomics*, 2014, 6, 1382-1386.
21. D. Gholap, J. Verhulst, W. Ceelen and F. Vanhaecke, *Anal Bioanal Chem*, 2012, 402, 2121-2129.
22. M. Bonta, H. Lohninger, V. Laszlo, B. Hegedus and A. Limbeck, *J. Anal. At. Spectrom.*, 2014, 29, 2159-2167.
23. K. Kanitsar, G. Koellensperger, S. Hann, A. Limbeck, H. Puxbaum and G. Stingeder, *J. Anal. At. Spectrom.*, 2003, 18, 239-246.
24. C. Paton, J. Hellstrom, B. Paul, J. Woodhead and J. Hergt, *J. Anal. At. Spectrom.*, 2011, 26, 2508.
25. http://iolite.earthsci.unimelb.edu.au/wiki/doku.php, Accessed 2014-05-15.
26. http://imagej.nih.gov/ij/.